

https://doi.org/10.1070/QEL18021

IR laser oscillation on caesium and rubidium atomic transitions upon pumping to high-lying energy levels

A.A. Babin, M.V. Volkov, S.G. Garanin, S.A. Kovaldov,
A.V. Kopalkin, F.A. Starikov, A.V. Strakhov, V.V. Feoktistov

Abstract. **Laser oscillation is obtained in caesium and rubidium atoms with wavelengths in the range of 2–5.5 μm under pumping to high-lying energy levels. Longitudinal resonant pumping is implemented using the second harmonic of radiation from an optical parametric oscillator. The pump wavelength is tuned over discrete levels from 8P to 10P in caesium atoms and from 6P to 8P in rubidium atoms. The width of the pump radiation spectrum is 12 cm^{-1}. When caesium atoms are pumped, the pump pulse energy is no more than 10 mJ; when rubidium atoms are pumped, it does not exceed 3 mJ. The pulse repetition rate is 10 Hz. The maximum output energy of IR laser radiation upon pumping the $9P_{3/2}$ level of caesium atoms is about 100 μJ at a cell temperature of ~170 °C, while the efficiency of pump conversion into radiation energy with a wavelength $\lambda \sim 3.1$ μm turns out to be ~1%. For rubidium atoms, an estimate of the output energy of IR radiation gives a value of ~80 μJ at a cell temperature of 180 °C, which corresponds to an energy efficiency of ~2.7%.**

Keywords: *laser, IR range, longitudinal pumping, atomic energy level structure, conversion efficiency.*

1. Introduction

As noted in Ref. [1], Cs and Rb atoms were among the first candidates for lasing in the optical, near, and mid-IR ranges, which is due to the well-developed energy level diagram of these metals. The first cw laser [2] based on caesium atoms was created two years later than the ruby laser [3], the launch of which gave rise to all laser physics. In [2], rather exotic pumping through helium atoms excited in a gas discharge was used. In this case, the energy of one of the strong emission lines of these atoms with $\lambda = 388.8$ nm resonantly populated the upper lasing energy level $8^2P_{1/2}$ of caesium atoms. Laser radiation with a wavelength of 7.18 μm was observed at the $8^2P_{1/2} \rightarrow 8^2S_{1/2}$ transition [2].

To date, laser oscillation has been obtained in caesium (Cs), rubidium (Rb), potassium (K), sodium (Na), and lithium (Li) atoms on $nP \rightarrow nS$ transitions, where $n = 6, 5, 4, 3, 2$ respectively [4]. We note that in these experiments, optical pumping by radiation of semiconductor laser diodes was used. Laser diodes have now become, first, commercially available, and, second, their characteristics (radiation linewidth and output power) make it possible to obtain a sufficiently high-power output laser radiation [5].

At the same time, it is of interest to obtain lasing in these atoms by pumping to higher energy levels. Here two aspects of research seem promising: 1) development of a new laser wavelength range; 2) classical spectroscopic interest associated with studying the migration of an excitation caused by a 'hard' optical photon, as well as with measuring the parameters of high-lying atomic transitions (e.g., the measurement of absorption cross sections and relaxation times of energy levels). The first part of these studies is of purely practical interest, associated, e.g., with laser applications such as optical location and ecology, while the second part is aimed at obtaining classical spectroscopic information about atoms.

In this paper, we study the possibility of lasing in the mid-IR range (2–5.5 μm) by exciting energy levels from 8P to 10P in caesium atoms and from 6P to 8P in rubidium atoms.

A technique is also proposed for measuring the absorption cross section σ_{mn} of these transitions for caesium and rubidium. This value was measured experimentally, and the values of σ_{mn} were compared with the calculated value for rubidium atoms, which showed good agreement with the experiment.

2. Schematic of the experimental setup

The layout of the experimental setup is completely similar to that used in [1]. We used the same tunable laser source of longitudinal pumping and the same scheme for detecting IR radiation emerging from a heated cell as in Ref. [1]. The difference in the design of the cell used for the excitation of rubidium vapour was that the cell windows were set at the Brewster angle for pump and output IR radiation. About 2 g of caesium or rubidium was placed in each cell, and a buffer gas ^{4}He was added at a pressure of 4 atm and room temperature, which improved the matching of the pump linewidth with the linewidth of the transition under study.

An alkali metal placed in a closed volume fills it with saturated vapours. To determine the concentration of saturated vapours of the rubidium isotope (^{85}Rb) and caesium (^{133}Cs) atoms, we used the results of Refs [6, 7], according to which the saturated vapour pressure above a substance can be determined from the formulas

$$\log_{10} p(T) = 4.046 - 3880/T \text{ for } ^{85}\text{Rb atoms}, \quad (1)$$

$$\log_{10} p(T) = 4.165 - 3830/T \text{ for } ^{133}\text{Cs atoms}, \quad (2)$$

A.A. Babin, M.V. Volkov, S.G. Garanin, S.A. Kovaldov, A.V. Kopalkin, F.A. Starikov, A.V. Strakhov, V.V. Feoktistov Federal State Unitary Enterprise 'Russian Federal Nuclear Centre – VNIIEF', prosp. Mira 37, 607188 Sarov, Nizhny Novgorod region, Russia;
e-mail: oefimova@otd13.vniief.ru, starikov@otd13.vniief.ru

Received 19 October 2021
Kvantovaya Elektronika **52** (4) 351–358 (2022)
Translated by V.L. Derbov

where pressure $p(T)$ is measured in physical atmospheres, and temperature T is measured in kelvins. The concentration of saturated vapours can be determined in terms of pressure and temperature according to the relation from Ref. [8]:

$$n = p/(k_B T), \quad (3)$$

where k_B is the Boltzmann constant.

As follows from Eqns (1)–(3), the concentration range of 10^{13}–10^{15} cm^{-3} is reached when the temperature changes from 90 to 190 °C for Cs and from 100 to 200 °C for Rb.

3. Spectral characteristics of a caesium vapour laser in the IR range

The study of the spectral composition of radiation during pumping of the energy levels $7P_{1/2,3/2}$ for caesium is thoroughly considered in Ref. [1]. Let us now consider which IR lasing lines are observed upon pumping the higher-lying 8P–10P energy levels.

3.1. Pumping the $8P_{1/2,3/2}$ energy levels

A study of the spectral composition of the generated radiation using an IR monochromator showed that, when caesium vapour was pumped to the $8P_{1/2,3/2}$ energy levels (λ_p = 388.8 and 387.55 nm, respectively), lasing occurred at the following transitions with the corresponding wavelengths:

1) $5D_{3/2} \rightarrow 6P_{1/2}$ (λ = 3013 nm);
2) $7P_{1/2} \rightarrow 7S_{1/2}$ (λ = 3096 nm);
3) $5D_{5/2} \rightarrow 6P_{3/2}$ (λ = 3495nm);
4) $4F_{7/2} \rightarrow 6D_{5/2}$ (λ = 5436 nm).

The correspondence between the measured wavelengths and generating transitions was established using the Grotrian diagram for caesium [9]. It should be noted that the generation line with a wavelength λ = 7.18 μm, observed in Ref. [2], was not recorded by us, since the leucosapphire windows of the cell did not transmit this radiation.

Experiments have shown that the sets of lines generated upon pumping to the $8P_{1/2}$ and $8P_{3/2}$ energy levels coincide. The accuracy of determining the wavelength in our experiments was determined by the used monochromator and amounted to ~1 nm, so that some discrepancy between the measured wavelengths and their reference values can be associated with both the calibration of the monochromator and tuning it to the line.

Comparing the obtained experimental results with the Grotrian diagram [9], we indicate the channels through which the upper lasing energy levels can be populated:

1) $5D_{3/2} \rightarrow 6P_{1/2}$ (λ = 3013 nm). The population of the $5D_{3/2}$ energy level corresponds to two possible channels:

a) $8P_{1/2,3/2} \rightarrow 8S_{1/2} \rightarrow 7P_{1/2} \rightarrow 5D_{3/2}$ (three-stage cascade);

b) $8P_{1/2,3/2} \rightarrow 6D_{3/2} \rightarrow 7P_{1/2} \rightarrow 5D_{3/2}$ (three-stage cascade).

2) $7P_{1/2} \rightarrow 7S_{1/2}$ (λ = 3096 nm). This lasing energy level can also be populated via two channels:

a) $8P_{1/2,3/2} \rightarrow 8S_{1/2} \rightarrow 7P_{1/2}$ (two-stage cascade);

b) $8P_{1/2,3/2} \rightarrow 6D_{3/2} \rightarrow 7P_{1/2}$ (two-stage cascade).

3) $5D_{5/2} \rightarrow 6P_{3/2}$ (λ = 3495 nm). Population of the $5D_{5/2}$ energy level can occur through the following channels:

a) $8P_{1/2,3/2} \rightarrow 8S_{1/2} \rightarrow 7P_{3/2} \rightarrow 5D_{5/2}$ (three-stage cascade);

b) $8P_{3/2} \rightarrow 6D_{3/2,5/2} \rightarrow 7P_{3/2} \rightarrow 5D_{5/2}$ or $8P_{1/2} \rightarrow 6D_{3/2} \rightarrow 7P_{3/2} \rightarrow 5D_{5/2}$ (three-stage cascade). Note that the $8P_{1/2} \rightarrow 6D_{5/2}$ transition is forbidden by the selection rules for the total angular momentum.

4) $4F_{7/2} \rightarrow 6D_{5/2}$ (λ = 5436 nm). This lasing channel requires additional discussion because the population of the upper lasing energy level $4F_{7/2}$ of the caesium atom is a rather complicated process, since the pumped energy levels $8P_{1/2,3/2}$ lie below the $7D_{3/2,5/2}$ term. The $4F_{7/2}$ energy level inversion can occur through the allowed chain of transitions $8P_{3/2} \rightarrow 7D_{5/2} \rightarrow 4F_{7/2}$, in which it is necessary to overcome the energy barrier at the first transition $8P_{3/2} \rightarrow 7D_{5/2}$. According to the Grotrian diagram for caesium [9], the value of this barrier is ΔE = 0.044 eV.

Possible mechanisms for passing through it are given below:

1. Overcoming the barrier due to heating of the medium. The magnitude of the required superheat can be estimated. According to Ref. [8], the average thermal energy of an atom is

$$E = 3k_B T/2, \quad (4)$$

from which one can easily determine the temperature increment

$$\Delta T = 2\Delta E/(3k_B). \quad (5)$$

As follows from Eqn (5), for ΔE = 0.044 eV, the overheating ΔT is ~340 °C, which is much higher than the temperature used in the experiment. Therefore, this possibility is hardly realisable.

2. Overcoming the barrier due to the decay of dimeric Cs_2 molecules, as was observed in Ref. [10]. In this process, the dimer molecule decomposes under the action of pumping into two Cs atoms, one of which appears in the $7D_{5/2}$ excited state and the other in the $6S_{1/2}$ ground state. The excited atom then transfers energy to the $4F_{7/2}$ energy level, as a result of which lasing occurs at the $4F_{7/2} \rightarrow 6D_{5/2}$ transition with a wavelength λ = 5436 nm.

3. Chemical reactions leading to the formation of molecular complexes, including dimers of alkali metals. These processes can be quite efficient, as was observed for rubidium in Ref. [11]. For example (see [11, 12]), the collision of excited caesium or rubidium atoms can lead to the reaction

$$Rb(nl) + Rb(5p) \rightarrow Rb^+ + Rb(5s) + e^-, \quad (6)$$

where Rb(nl) is rubidium at highly excited energy levels (nl = 6D, 8S, or 7D); and Rb(5p) is the rubidium atom at the 5P energy level. As a result, an ionised rubidium atom Rb^+, a rubidium atom in the 5S ground state, and a free electron e^- appear. Moreover, the cross section for this reaction is large (6×10^{-13} cm^2) [11]. For the caesium atom, the reaction cross section has the same order [11, 12]. A charged alkali metal ion easily forms a dimer molecule (Rb_2 or Cs_2), which, upon decay according to the scenario given in step 2 above, leads to lasing at the transition $4F_{7/2} \rightarrow 6D_{5/2}$ for caesium atoms.

It should be noted that the cell temperature at which lasing occurred at the strongest $7P_{1/2} \rightarrow 7S_{1/2}$ transition, λ = 3096 nm (actually the threshold temperature) upon pumping to the $8P_{1/2,3/2}$ energy levels, was 110–115 °C. In this case, the energy fluctuation of the output IR radiation, which arises due to the instability of the output pump energy (~5%), exceeded 100% as before [1]. With a further increase in the cell temperature, the spread of the output energy of the IR

signal stabilised at the level of 10%–12%. Misalignment of the highly reflective resonator mirror at a cell temperature of ~180 °C led to a more than 10-fold decrease in the output signal. Therefore, cavity generation of IR radiation in caesium vapour is evident.

3.2. Pumping the $9P_{1/2,3/2}$ energy levels

A series of experiments to study the spectral characteristics of laser radiation from caesium atoms was carried out with pumping of the 9P energy levels. When the $9P_{1/2}$ and $9P_{3/2}$ energy levels were pumped (λ_p = 361.7 and 361.14 nm, respectively), lasing in the range of 2–5.5 μm was observed at the following transitions with the corresponding wavelengths:

1) $9P_{1/2} \rightarrow 8S_{1/2}$ (λ = 3025 nm);
2) $8P_{3/2} \rightarrow 6D_{3/2}$ (λ = 3110 nm);
3) $5D_{5/2} \rightarrow 6P_{3/2}$ (λ = 3495 nm);
4) $5G_{9/2} \rightarrow 4F_{7/2}$ (λ = 3960 nm);
5) $4F_{7/2} \rightarrow 6D_{5/2}$ (λ = 5436 nm).

The emitted wavelengths were identified in the same way as in the previous cases. Let us now consider the channels through which the upper lasing energy levels can be populated:

1) $9P_{1/2} \rightarrow 8S_{1/2}$ (λ = 3025 nm) – direct laser transition.

2) $8P_{3/2} \rightarrow 6D_{3/2}$ (λ = 3110 nm). Population of the upper lasing energy level $8P_{3/2}$ can occur through two channels:

a) $9P_{1/2,3/2} \rightarrow 9S_{1/2} \rightarrow 8P_{3/2}$ (two-stage cascade);

b) $9P_{3/2} \rightarrow 7D_{3/2,5/2} \rightarrow 8P_{3/2}$ or $9P_{1/2} \rightarrow 7D_{3/2} \rightarrow 8P_{3/2}$ (two-stage cascade), the transition $9P_{1/2} \rightarrow 7D_{5/2}$ is prohibited by the selection rules.

3) $5D_{5/2} \rightarrow 6P_{3/2}$ (λ = 3495 nm). Population of the $5D_{5/2}$ energy level is possible through three channels:

a) $9P_{1/2,3/2} \rightarrow 9S_{1/2} \rightarrow 7P_{3/2} \rightarrow 5D_{5/2}$ (three-stage cascade);

b) $9P_{3/2} \rightarrow 7D_{3/2,5/2} \rightarrow 7P_{3/2} \rightarrow 5D_{5/2}$ or $9P_{1/2} \rightarrow 7D_{3/2} \rightarrow 7P_{3/2} \rightarrow 5D_{5/2}$ (three-stage cascade);

c) $9P_{1/2,3/2} \rightarrow 7D_{3/2,5/2} \rightarrow 4F_{5/2,7/2} \rightarrow 5D_{5/2}$ (three-stage cascade). Note that the $9P_{1/2} \rightarrow 7D_{5/2}$ and $7D_{3/2} \rightarrow 4F_{7/2}$ transitions are forbidden by the selection rules for the total angular momentum.

4) $5G_{9/2} \rightarrow 4F_{7/2}$ (λ = 3960 nm). Population of this energy level is possible through the following channels:

a) $9P_{3/2} \rightarrow 8D_{5/2} \rightarrow 6F_{7/2} \rightarrow 5G_{9/2}$;

b) $9P_{3/2} \rightarrow 8D_{5/2} \rightarrow 5F_{7/2} \rightarrow 5G_{9/2}$.

As follows from the Grotrian diagram and previous considerations, to obtain lasing with a wavelength of 3960 nm upon excitation of caesium atoms to the energy levels $9P_{1/2,3/2}$, it is necessary to populate the $5G_{9/2}$ energy level. This is possible through the two channels presented above (4a and 4b). However, in both channels it is necessary to overcome two energy barriers: at the first and second transitions for channel 4a and at the first and third transitions for channel 4b. Channel 4a is probably not implemented, since the first $9P_{3/2} \rightarrow 8D_{5/2}$ transition requires a temperature of ~120 °C, while the $8D_{5/2} \rightarrow 6F_{7/2}$ transition requires a temperature of ~480 °C. Correspondingly, for channel 4b, the necessary overheating values ΔT are 120 °C (the first transition $9P_{3/2} \rightarrow 8D_{5/2}$) and 54 °C (the third transition $5F_{7/2} \rightarrow 5G_{9/2}$). Consequently, channel 4b can be realised, which will lead to the inversion at the $5G_{9/2}$ energy level and, accordingly, to lasing at a wavelength of 3960 nm.

5) $4F_{7/2} \rightarrow 6D_{5/2}$ (λ = 5436 nm). Population of the upper lasing energy level is possible via the $9P_{3/2} \rightarrow 7D_{5/2} \rightarrow 4F_{7/2}$ channel or through the formation and subsequent decay of dimeric Cs_2 molecules (similarly to [10]).

3.3. Pumping the $10P_{1/2,3/2}$ energy levels

As for the excitation of the $10P_{1/2,3/2}$ energy level upon its pumping by radiation with wavelengths λ_p = 348.0 and 347.7 nm, respectively, in the range 2–5.5 μm, a single laser line with λ = 3096 nm was observed (transition $7P_{1/2} \rightarrow 7S_{1/2}$). Possibly, this is because pumping at such a wavelength is beyond the absorption band of Cs_2 molecular complexes, as a result of which their decay does not occur during the action of a short pulse. The mechanism for producing an inversion at the upper lasing energy level $7P_{1/2}$ is most likely a two-stage process $10P_{1/2,3/2} \rightarrow 9S_{1/2} \rightarrow 7P_{1/2}$ or more complex multi-stage chains like $10P_{1/2,3/2} \rightarrow 10S_{1/2} \rightarrow 9P_{1/2} \rightarrow 9S_{1/2} \rightarrow 8P_{1/2} \rightarrow 8S_{1/2} \rightarrow 7P_{1/2}$. All such multistage energy transfer processes lead to the inversion at the $7P_{1/2} \rightarrow 7S_{1/2}$ transition.

4. Energy characteristics of a caesium vapour laser in the IR range

For all excited energy levels of the Cs atom, from $8P_{1/2,3/2}$ to $10P_{1/2,3/2}$, maximally attainable for our setup, we measured the dependences of the cell transmittance on temperature $K(T)$, as well as the temperature dependences of the relative energy per pulse in the IR range.

The cell transmittance was defined as follows:

$$K = W_{tr}/W_{in}, \tag{7}$$

where W_{tr} is the pump energy that passed through the cell with Cs vapour; and W_{in} is the energy at the input to the cell.

Since the dependences obtained turned out to be of the same type for all the analysed transitions in caesium atoms, as examples we present the dependences of the cell transmittance $K(T)$ (Fig. 1) and the IR signal energy $W(T)$ (Fig. 2) on temperature during pumping to $9P_{1/2,3/2}$ energy levels. It can be seen from Fig. 1 that the pump energy of a higher-lying sublevel is absorbed stronger and the operating range for its effective absorption begins at lower temperatures, while a higher temperature ($T > 200$ °C) is required for efficient conversion of the pump energy of the lower-lying $9P_{1/2}$ transition to the IR range.

According to Fig. 2, lasing upon pumping to the $9P_{1/2}$ energy level begins at a temperature of ~145 °C, and the highest lasing pulse energy is reached at temperatures of 180–190 °C.

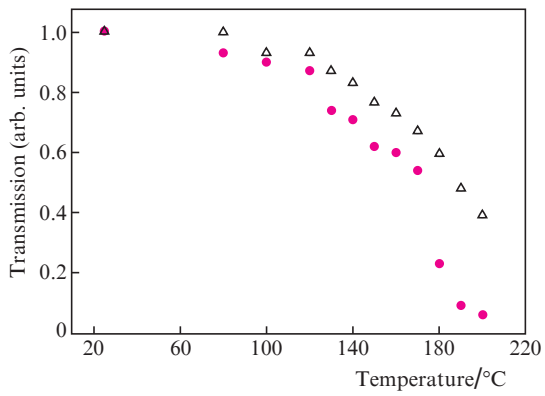

Figure 1. Temperature dependences of cell transmission under pumping to the $9P_{1/2}$ (triangles) and $9P_{3/2}$ (circles) energy levels for Cs atoms.

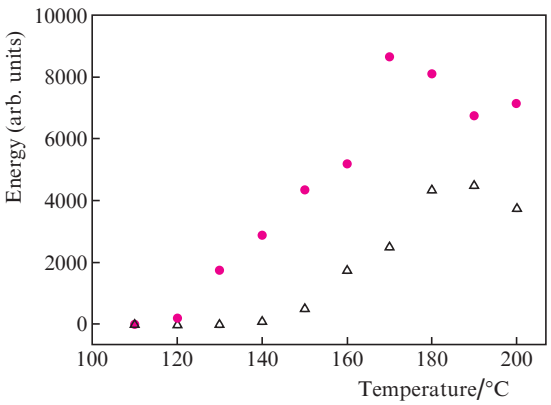

Figure 2. Dependences of the laser pulse energy at a wavelength of 3.1 μm on temperature under pumping to the energy levels $9P_{1/2}$ (triangles) and $9P_{3/2}$ (circles) for Cs atoms.

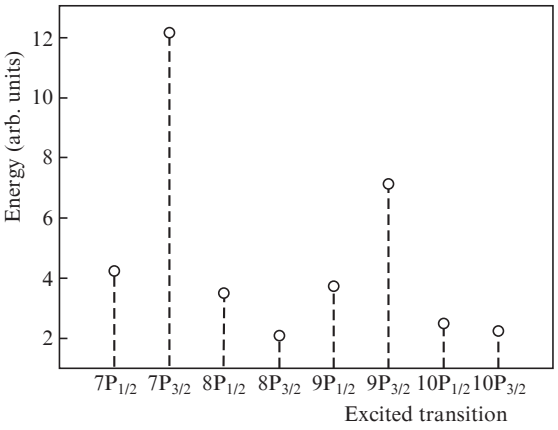

Figure 3. Highest energies in a laser pulse with a wavelength of ~3.1 μm under pumping to the 7P–10P energy levels for Cs atoms.

Upon pumping to the $9P_{3/2}$ energy level, lasing starts at a lower temperature (~120 °C) than upon pumping to the $9P_{1/2}$ energy level and reaches its maximum value already at a temperature of ~165 °C. A characteristic change in the shape of the spectral line of the past pumping ('depletion') occurs at a temperature of ~150 °C. Such a temperature difference for different pumping is probably related to the different parameters of the excited $9P_{1/2}$ and $9P_{3/2}$ energy levels.

Since all experiments were carried out under the same conditions for receiving radiation from the output of the monochromator, the ordinates of the dependences for the wavelength $\lambda = 3110$ nm can be compared with each other. It also follows from Fig. 2 that the maximum energy in an IR pulse is higher when pumping to the $9P_{3/2}$ energy level.

When the $10P_{1/2,3/2}$ energy levels ($\lambda_p = 348.0$ and 347.7 nm, respectively) were pumped in the range of 2–5.5 μm, as already noted, a single lasing line was observed with a wavelength $\lambda = 3096$ nm (transition $7P_{1/2} \rightarrow 7S_{1/2}$). When pumped to these energy levels, similar temperature dependences of the energy transmission coefficients of the cell were obtained, and for the generating line, the dependence of the signal magnitude on temperature was obtained.

Let us summarise the data on the strongest generation line with a wavelength of ~3.1 μm upon pumping to different energy levels, including the data obtained in Ref. [1]. The results are shown in Fig. 3, from which it follows that the highest energy in an IR pulse with a wavelength $\lambda \sim 3.1$ μm was obtained at the $7P_{1/2} \rightarrow 7S_{1/2}$ transition when pumped to the $7P_{3/2}$ energy level ($\lambda_p = 455.5$ nm). Upon pumping to the $9P_{3/2}$ energy level, the resulting energy in the generation pulse is 1.7 times lower.

5. Spectral characteristics of a rubidium vapour laser in the IR range

The main and essential difference of lasing in rubidium vapour from that in caesium vapour was revealed in the very first experiments. It turned out that for a cell with rubidium, the magnitude of the IR signals does not depend on the presence of resonator mirrors, for which we used a highly reflective dielectric mirror, and a leucosapphire substrate (Al_2O_3) that served as the output mirror. An attempt to install an output mirror with higher reflection was not successful due to the optical destruction of the reflective surface. Thus, single-pass generation of IR radiation occurs in rubidium vapour, rather than cavity lasing, as was the case for caesium. In fact, in this case, we are dealing with stimulated Raman scattering, in which there is no need to place the active medium in a cavity since laser radiation arises due to convective instability in the active medium. We also note that in experiments with rubidium, we did not observe a 'dip' in the spectrum of transmitted pump radiation for any of the excited energy levels, as in the case of pumping the energy levels of caesium atoms.

Identification of the recorded wavelengths of IR radiation during pumping of rubidium vapour was also carried out using the Grotrian diagram taken from Ref. [9].

5.1. Pumping the $6P_{1/2,3/2}$ energy levels

Study of the spectral composition of radiation during pumping of the $6P_{1/2}$ and $6P_{3/2}$ energy levels(λ_p = 421.6 and 420.2 nm, respectively), the energy separation between which is 77.5 cm^{-1}, or 0.0096 eV [9], showed that three different sets of wavelengths were generated for both pumps.

When pumping to the upper sublevel $6P_{3/2}$:

1) $6P_{3/2} \rightarrow 4D_{5/2}$ ($\lambda_p = 2250$ nm);
2) $6P_{3/2} \rightarrow 6S_{1/2}$ ($\lambda_p = 2730$ nm);
3) $6P_{1/2} \rightarrow 6S_{1/2}$ ($\lambda_p = 2790$ nm).

When pumping to the lower sublevel $6P_{1/2}$:

1) $6P_{3/2} \rightarrow 4D_{5/2}$ ($\lambda_p = 2250$ nm);
2) $6P_{1/2} \rightarrow 4D_{3/2}$ ($\lambda_p = 2290$ nm);
3) $6P_{1/2} \rightarrow 6S_{1/2}$ ($\lambda_p = 2790$ nm).

All observed generation lines are direct transitions.

It should be noted that in these experiments a collisional 'mixing' of the $6P_{1/2}$ and $6P_{3/2}$ sublevels was observed, since the radiative transition between them is forbidden by the selection rules. We observed the $6P_{1/2} \rightarrow 6S_{1/2}$ lasing line when the upper $6P_{3/2}$ sublevel was pumped, and vice versa, when the lower $6P_{1/2}$ sublevel was pumped, lasing occurred at the $6P_{3/2} \rightarrow 4D_{5/2}$ transition. This means that the process of collisional 'mixing' of the $6P_{1/2}$ and $6P_{3/2}$ sublevels is rather fast and efficient, since an inversion occurs in the transitions $6P_{1/2} \rightarrow 6S_{1/2}$ and $6P_{3/2} \rightarrow 4D_{5/2}$, and they have time to generate at such a short pump pulse (in the experiment, at an operating cell temperature of ~150 °C, the buffer gas pressure increased to 4.5 atm). Thus, we can assume that the 'mixing' time of the $6P_{1/2,3/2}$ sublevels at a temperature of ~150 °C is less than a nanosecond.

5.2. Pumping the $7P_{1/2,3/2}$ energy levels

A series of experiments to study the spectral characteristics of rubidium atoms was also carried out upon pumping the 7P energy levels. When the $7P_{1/2}$ and $7P_{3/2}$ energy levels were pumped (λ_p = 359.2 and 358.7 nm, respectively), lasing in the range 2–5.5 μm was observed at transitions with the following wavelengths:

1) $6P_{3/2} \rightarrow 4D_{5/2}$ (λ_p = 2250 nm);
2) $6P_{3/2} \rightarrow 6S_{1/2}$ (λ_p = 2730 nm).

In contrast to pumping the 6P energy levels, the sets of generated lines upon pumping the $7P_{1/2}$ and $7P_{3/2}$ energy levels coincide. It should be noted that the magnitude of the signal of the recorded lines turned out to be smaller than when pumped to the 6P energy levels. This is due to the fact that, upon pumping to the $7P_{1/2}$ and $7P_{3/2}$ energy levels, the upper lasing energy level $6P_{3/2}$ is populated in a two-stage cascade as follows: $7P_{1/2,3/2} \rightarrow 5D_{3/2} \rightarrow 6P_{3/2}$, or $7P_{3/2} \rightarrow 5D_{5/2} \rightarrow 6P_{3/2}$.

Another two-stage cascade, $7P_{1/2,3/2} \rightarrow 7S_{1/2} \rightarrow 6P_{3/2}$, is not realised, since in this case, the transition $7S_{1/2} \rightarrow 6P_{3/2}$ must (as will be shown below) lead to the generation of a line with λ = 4.0 μm. However, this wavelength was not observed in the experiment. Therefore, pumping the energy levels $7P_{1/2,3/2}$ of rubidium leads to lasing with two wavelengths.

5.3. Pumping the $8P_{1/2,3/2}$ energy levels

When pumping the $8P_{1/2}$ and $8P_{3/2}$ energy levels (λ_p = 335.09 and 334.87 nm, respectively) in the range of 2–5.5 μm, a single line was obtained with a wavelength λ = 4.0 μm, which is generated on transition $7S_{1/2} \rightarrow 6P_{3/2}$. Population of the upper lasing energy level $7S_{1/2}$ is possible through the following channels:

a) $8P_{1/2,3/2} \rightarrow 8S_{1/2} \rightarrow 7P_{1/2,3/2} \rightarrow 7S_{1/2}$ (three-stage cascade);

b) $8P_{1/2,3/2} \rightarrow 6D_{3/2,5/2} \rightarrow 7P_{1/2,3/2} \rightarrow 7S_{1/2}$ (three-stage cascade). Note that the transitions $8P_{1/2} \rightarrow 6D_{5/2}$ and $6D_{5/2} \rightarrow 7P_{1/2}$ are forbidden by the selection rules for the total angular momentum.

We could not observe other possible longer-wavelength lasing lines (e.g., the $8P_{1/2,3/2} \rightarrow 8S_{1/2}$ transitions, λ = 12.677 and 12.423 μm, respectively) with our setup, because we used leucosapphire cell windows transparent in the IR range up to about 5.75 μm.

6. Energy characteristics of a rubidium vapour laser in the IR range

Similar to the experiments with caesium vapour, in all experiments performed with rubidium vapour, we determined the dependences of the cell transmittance and the generated relative energy per pulse on temperature when pumped to all energy levels 6P, 7P, and 8P achievable in our experiment. It should be noted that in contrast to the case of similar dependences for caesium, in all the experiments performed, the dependences obtained upon pumping to the upper ($nP_{3/2}$) and lower ($nP_{1/2}$) sublevels turned out to be significantly different upon excitation of the 6P, 7P, and 8P energy levels. Therefore, we present the experimental results for each of them.

Figure 4 shows the dependence of the cell transmittance $K(T)$ on pumping of the $6P_{1/2}$ and $6P_{3/2}$ energy levels. It can be seen that the dependences obtained for both sublevels practically coincide. This circumstance corresponds to the temperature dependences of the output energy in the generated pulse. It follows from Fig. 5 that when pumping to different sublevels of the 6P term, the generation of IR radiation begins at approximately the same temperatures, despite the difference in the emitted wavelengths (here, the signals can also be compared).

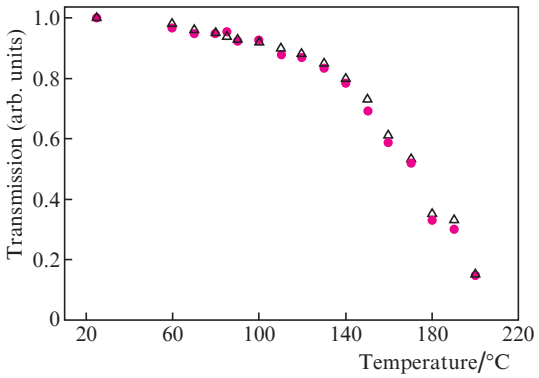

Figure 4. Temperature dependences of the cell transmission under pumping to the $6P_{1/2}$ (triangles) and $6P_{3/2}$ (circles) energy levels for Rb atoms.

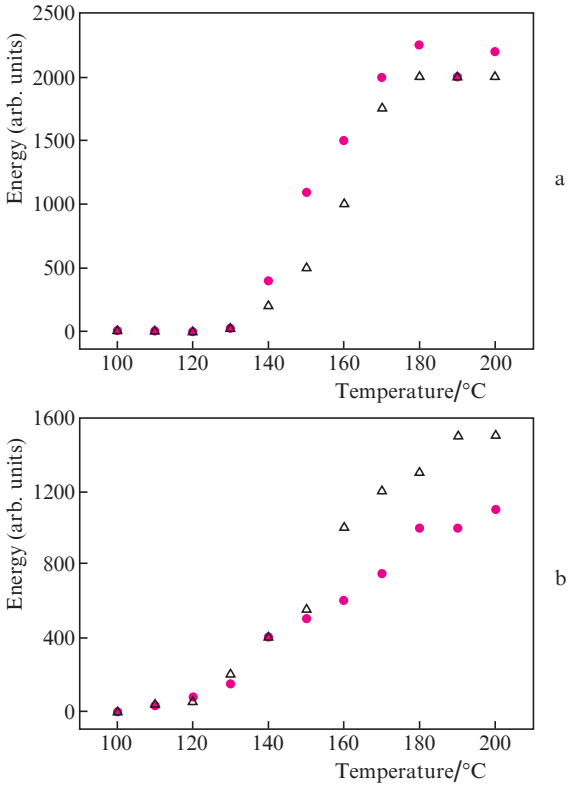

Figure 5. Temperature dependences of the energies in a laser pulse with λ = (a) 2.25 and (b) 2.79 μm pumped to the $6P_{1/2}$ (triangles) and $6P_{3/2}$ (circles) energy levels for Rb atoms.

Figure 6 shows the temperature dependence of the transmittance $K(T)$ when pumping the $7P_{1/2}$ and $7P_{3/2}$ energy levels. In this case, the dependences obtained differ from the previous case, namely, the absorption of the pump to the upper $7P_{3/2}$ sublevel begins at lower temperatures than for pumping to the $7P_{1/2}$ energy level. In addition, pump absorption of

~90% in the cell occurs at a temperature difference of about 30 °C. This means that saturation of the temperature dependence of the generation energy should occur earlier when pumping to the $7P_{3/2}$ sublevel, as was observed in the experiment (Fig. 7). It also follows from Fig. 7 that the maximum energies of IR pulses when pumping both sublevels for wavelengths $\lambda = 2250$ and 2730 nm coincide.

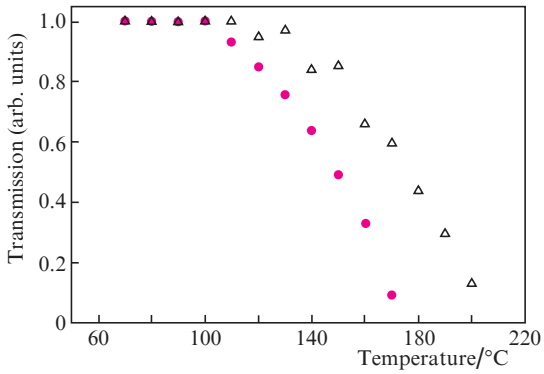

Figure 6. Temperature dependences of the cell transmission under pumping to the $7P_{1/2}$ (triangles) and $7P_{3/2}$ (circles) energy levels for Rb atoms.

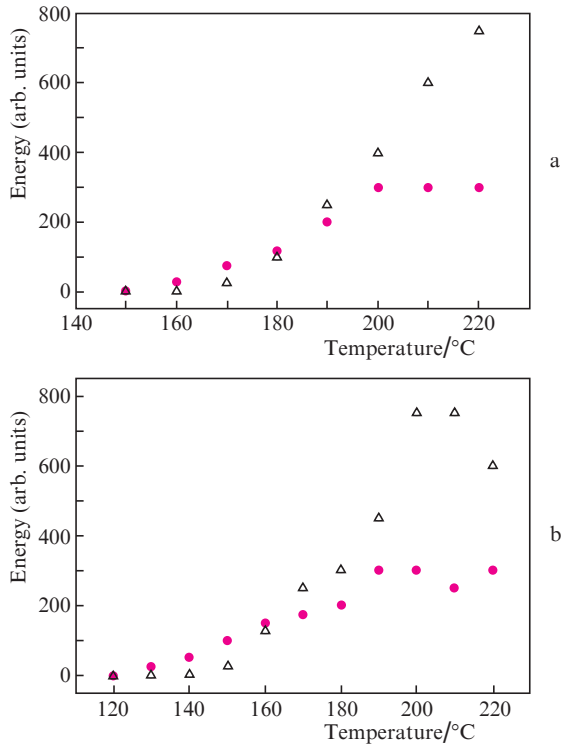

Figure 7. Dependences of the energies in the laser pulse under pumping to (a) $7P_{1/2}$ and (b) $7P_{3/2}$ energy levels [$\lambda = 2.25$ (triangles) and 2.73 μm (circles)] on temperature for Rb atoms.

When pumped to the 8P energy levels, the temperature dependences of the transmittance are shown in Fig. 8a. As follows from this figure, the temperature at which lasing begins is inverted compared to the previous case (pumping to 7P energy levels). It can be seen from Fig. 8b that saturation of the generation energy for the $8P_{1/2}$ sublevel is achieved at

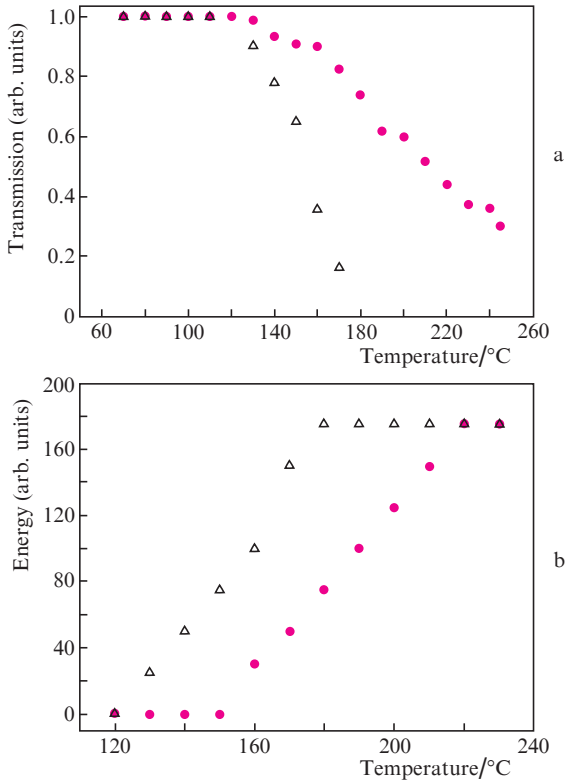

Figure 8. Dependences of (a) the cell transmission and (b) the energy in the generation pulse ($\lambda = 4$ μm) on temperature under pumping to the energy levels $8P_{1/2}$ (triangles) and $8P_{3/2}$ (circles) for Rb atoms.

significantly lower temperatures (~180 °C) than for the $8P_{3/2}$ sublevel (~220 °C).

Summarising the energy results, we can say that the highest energy of IR radiation was obtained by pumping to the $6P_{3/2}$ energy level ($\lambda_p = 420.2$ nm). For this case, Fig. 9 shows the oscillogram of the generation pulse obtained using a FSG-22-3A2 photoresistor, from which it is possible to estimate the generated IR pulse duration, as well as the total energy of IR components generated in the cell, using the volt-watt characteristic of the detector (the nominal being 1300 V W^{-1}). An estimate based on this characteristic gives an IR pulse energy of ~80 μJ. In this case, the pump energy was ~3 mJ. Therefore, the estimated energy efficiency is ~2.7%. It should

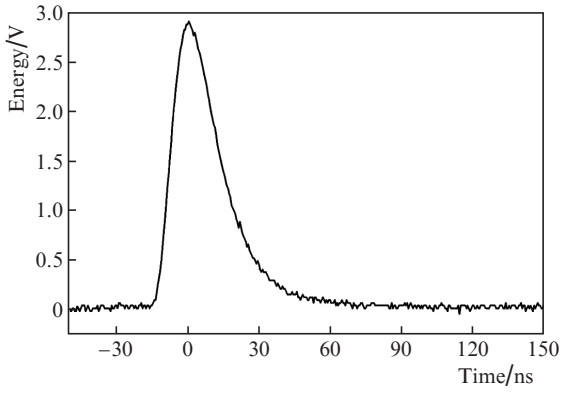

Figure 9. Time dependence of the total signal energy in the oscillation pulse under pumping to the $6P_{3/2}$ energy level for Rb atoms.

also be noted that the temporal shape of the generation pulse shown in Fig. 9 differs markedly from the similar shape for caesium, since it has no spike structure characteristic of cavity lasing, as was observed in Ref. [1].

We note that resonator-free lasing in the three-micron range in rubidium vapour was obtained in Ref. [13] at an output energy of $\sim 100 \times 10^{-9}$ J; however, the pump conversion efficiency was extremely low (it was estimated in Ref. [13] at the level of 10^{-4}). In our experiments, we managed to obtain an almost three orders of magnitude higher conversion efficiency to IR radiation.

7. Measurement of the absorption cross section for high-lying transitions in caesium and rubidium atoms

Our measurements allow us to obtain another important information concerning the spectroscopic characteristics of high-lying transitions in caesium and rubidium atoms. We are talking about such a parameter as the absorption cross section of the transition. This characteristic can be extracted from the analysis of the temperature dependence of the cell transmittance. Indeed, according to the Bouguer–Lambert–Beer law [8], the intensity of a monochromatic signal at the sample output is

$$I_1 = I_0 \exp(-\alpha), \tag{8}$$

where I_0 is the intensity of radiation incident on the cell; $\alpha = \sigma n l$ is the absorption coefficient; σ is the desired cross section (cm^2); n is the concentration of absorbing atoms (cm^{-3}); and l is the cell length (cm). Then the transmittance is expressed as

$$K = I_1/I_0 = \exp(-\alpha). \tag{9}$$

Therefore,

$$\sigma = -\ln(K)/nl. \tag{10}$$

Taking the transmission coefficient $K(T)$ equal to 95% (in this case, we have a small pump absorption at which the entire length of the cell should work), from the measured $K(T)$ dependence we find the temperature of atoms in the cell, $T_{0.95}$, corresponding to this transmission. Then, and according to Eqns (1)–(3) we find the concentration of caesium or rubidium atoms, n. Now all the quantities necessary to find the absorption cross section are determined and, consequently, the value of σ itself can be found from expression (10).

Let us also determine the error of the result obtained using the relation

$$\Delta\sigma = \sqrt{\left(\frac{\partial\sigma}{\partial K}\frac{\partial K}{\partial T}\Delta T\right)^2 + \left(\frac{\partial\sigma}{\partial n}\frac{\partial n}{\partial T}\Delta T\right)^2}. \tag{11}$$

The absorption cross sections found in this way for various transitions are given in Tables 1 and 2 for caesium and rubidium atoms. The errors calculated using Eqn (11) are also given there.

Note that the data given in Table 1 for the $6S_{1/2} \rightarrow 7P_{1/2}$ and $6S_{1/2} \rightarrow 7P_{3/2}$ transitions were found from the results of Ref. [1].

It should be noted that the obtained values of σ are lower bounds, since expression (10), strictly speaking, is valid only for monochromatic pump radiation. In our experiments, the width of the pump line is approximately equal to the width of the emission line, and, therefore, we measured certain quantities averaged over the spectrum, which should give a smaller absorption cross section σ. This circumstance can be taken into account by averaging σ over the pump spectrum.

Table 1. Absorption cross sections for the investigated transitions in the caesium atom.

Transition	T/°C	$n/10^{13}$ cm^{-3}	$\sigma/10^{-16}$ cm^2	$\Delta\sigma/10^{-16}$ cm^2
$6S_{1/2} \rightarrow 7P_{1/2}$	70	0.3	3.42	0.39
$6S_{1/2} \rightarrow 7P_{3/2}$	75	0.4	2.56	0.30
$6S_{1/2} \rightarrow 8P_{1/2}$	120	7	0.15	0.02
$6S_{1/2} \rightarrow 8P_{3/2}$	110	4	0.26	0.03
$6S_{1/2} \rightarrow 9P_{1/2}$	125	8	0.13	0.02
$6S_{1/2} \rightarrow 9P_{3/2}$	90	0.9	1.14	0.13
$6S_{1/2} \rightarrow 10P_{1/2}$	140	20	0.05	0.01
$6S_{1/2} \rightarrow 10P_{3/2}$	115	5	0.21	0.02

Table 2. Absorption cross sections for the studied transitions in the rubidium atom.

Transition	T/°C	$n/10^{13}$ cm^{-3}	$\sigma/10^{-16}$ cm^2	$\Delta\sigma/10^{-16}$ cm^2
$5S_{1/2} \rightarrow 6P_{1/2}$	70	0.2	5.13	0.57
$5S_{1/2} \rightarrow 6P_{3/2}$	70	0.2	5.13 (measured) 20 (calculated at the line centre)	0.57
$5S_{1/2} \rightarrow 7P_{1/2}$	110	1.5	0.68	0.08
$5S_{1/2} \rightarrow 7P_{3/2}$	120	3	0.34	0.04
$5S_{1/2} \rightarrow 8P_{1/2}$	140	8	0.13	0.01
$5S_{1/2} \rightarrow 8P_{3/2}$	130	6	0.17	0.02

It is known [14] that the absorption cross section can be calculated from the formula

$$\sigma_{abs} = \frac{g_2}{g_1}\frac{\lambda^2}{8\pi}A_{21}g(\nu), \tag{12}$$

where g_1 and g_2 are the degeneracy multiplicities of the energy levels; λ is the pump wavelength for a given transition; A_{21} is the Einstein coefficient for spontaneous emission, equal to the reciprocal lifetime τ of the upper laser energy level; and $g(\nu)$ is the spectral line shape function.

For the $5S_{1/2} \rightarrow 6P_{3/2}$ transition in the rubidium atom, the lifetime τ of the upper laser energy level [15] and the collisional broadening coefficients γ [16] are known; therefore, the theoretical value of the absorption cross section at the absorption maximum can be estimated. Since the medium is dominated by collisional broadening, which is homogeneous [14], then $g(\nu)$is the Lorentz function [14]:

$$g(\nu) = \frac{1}{2\pi}\frac{\Delta\nu_{las}}{(\nu-\nu_0)^2 + (\Delta\nu_{las}/2)^2}, \tag{13}$$

where ν_0 is the frequency at the absorption line centre (pump frequency); $\Delta\nu_{las} = \Delta\nu_{col} = \gamma p$ is the collisional broadening width. At the centre of the line, i.e., at $\nu = \nu_0$,

$$g(\nu_0) = \frac{2}{\pi}\frac{1}{\Delta\nu_{las}} \approx \frac{0.637}{\Delta\nu_{las}}. \tag{14}$$

According to Refs [15, 16], for the $5S_{1/2} \rightarrow 6P_{3/2}$ transition, the lifetime is $\tau = 357$ ns, $g_1 = 2$, $g_2 = 4$, $\gamma =$

48.8 MHz Torr^{-1}. Then the absorption cross section at the centre of the line is

$$\sigma_{abs}(\nu_0) \approx 2 \times 10^{-15}\ \text{cm}^2. \quad (15)$$

The calculated value of σ_{abs} corresponds to the centre of the absorption line and is approximately four times larger than the measured one. If the Lorentz function (13) is averaged over the frequency ν, then we obtain the value $\overline{g(\nu)}$ averaged over the spectrum, which corresponds to the absorption measured in the experiment. For the averaging range $\Delta\nu$ = 0.25 nm, which corresponds to the width of the pump emission line, the calculated value of $\overline{g(\nu)}$ decreases by about four times and (taking the error into account) practically coincides with the measured value of σ. This allows us to hope that all other experimental values of the absorption cross sections in caesium and rubidium atoms, measured by the method described above, should be correct.

8. Conclusions

Thus, the studies performed have demonstrated the possibility of cavity lasing in the IR range (3–5.5 μm) upon excitation of high-lying energy levels of caesium atoms (8P, 9P, and 10P), as well as resonator-free lasing (essentially, SRS generation) in range of 2.25–4 μm upon excitation of high-lying energy levels of rubidium atoms. The efficiency of conversion of pump energy into IR pulse energy for caesium is ~1% ($8P_{3/2} \rightarrow 6D_{3/2}$ transition, λ = 3.1 μm). For rubidium atoms, the estimate of the energy conversion efficiency is ~2.7% (transition $6P_{3/2} \rightarrow 4D_{5/2}$, λ = 2.25 μm).

For rubidium atoms, the effect of mixing of the $6P_{1/2}$ and $6P_{3/2}$ sublevels was also observed, which allowed estimating the time behaviour of this process.

A method has been proposed and implemented for measuring the absorption cross section of highly excited transitions in Cs and Rb atoms using quasi-monochromatic pumping whose spectrum width is comparable to that of the line under study.

References

1. Babin A.A., Volkov M.V., Garanin S G., et al. *Quantum Electron*., **51** (5), 415 (2021) [*Kvantovaya Elektron*., **51** (5), 415 (2021)].
2. Rabinowitz P., Jacobs S., Gould G. *Appl. Opt*., **1** (4), 513 (1962).
3. Maiman T.N. *Nature*, **187**, 493 (1960).
4. Shalagin A.M. *Phys. Usp*., **54**, 975 (2011) [*Usp. Fiz. Nauk*, **181**, 1011 (2011)].
5. Bogachev A.V., Garanin S.G., Dudov A.M., et al. *Quantum Electron*., **42** (2), 95 (2012) [*Kvantovaya Elektron*., **42** (2), 95 (2012)].
6. Plushev V.E., Stepin B.D. *Khimiya i tekhnologiya soedinenii litiya, rubidiya i tseziya* (Chemistry and Technology of Lithium, Rubidium and Caesium Compounds) (Moscow: Khimiya, 1970) p. 75.
7. Steck D.A. http://steck.us/alkalidata (revision 2.1.2, 12 August 2009).
8. Detlaf A.A., Yavorsky B.M. *Kurs fiziki* (Physics Course) (Moscow: Vysshaya shkola, 1973) Vol. I, p. 270.
9. Grigoriev I.S., Meilikhov E.Z. (Eds) *Handbook of Physical Quantities* (Boca Raton: CRC Press, 1997; Moscow: Energoatomizdat, 1991).
10. Sitnikov M.G., Znamenskii N.V., et al. *Quantum Electron*., **30** (3), 221 (2000) [*Kvantovaya Elektron*., **30** (3), 221 (2000)].
11. Barbier L., Cheret M. *J. Phys. B: At. Mol. Phys*., **20**, 1229 (1987).
12. Barbier L., Cheret M. *J. Phys. B: At. Mol. Phys*., **16**, 3213 (1983).
13. Moran P.J., Richards R.M., et al. *Opt. Commun*., **374**, 51 (2016).
14. Svelto O. *Principles of Lasers* (New York: Plenum Publishing Co., 1989).
15. Heavens O.S. *J. Opt. Soc. Am*., **51** (10), 1058 (1961).
16. Aumiler D., Ban T., Pichler G. *Phys. Rev. A*, **70**, 032723 (2004).